

Energy storage performances regulated by $BiMnO_3$ proportion in limited solid solution films

Fei Guo(郭飞), Zhifeng Shi(史智锋), Yaping Liu(刘亚平), Shifeng Zhao(赵世峰)

Citation: Chin. Phys. B . 2020, 29(11): 116801 . **doi:** 10.1088/1674-1056/aba604
Journal homepage: http://cpb.iphy.ac.cn; http://iopscience.iop.org/cpb

What follows is a list of articles you may be interested in

Influence comparison of N_2 and NH_3 nitrogen sources on AlN films grown by halide vapor phase epitaxy

Jing-Jing Chen(陈晶晶), Jun Huang(黄俊), Xu-Jun Su(苏旭军), Mu-Tong Niu(牛牧童), Ke Xu(徐科)

Chin. Phys. B . 2020, 29(7): 076802 . **doi:** 10.1088/1674-1056/ab90ed

Growth and aggregation of Cu nanocrystals on ionic liquid surfaces

Jia-Wei Shen(沈佳伟), Xun-Heng Ye(叶迅亨), Zhi-Long Bao(鲍志龙), Lu Li(李璐), Bo Yang(杨波), Xiang-Ming Tao(陶向明), Gao-Xiang Ye(叶高翔)

Chin. Phys. B . 2020, 29(6): 066801 . **doi:** 10.1088/1674-1056/ab8896

Growth and transport properties of topological insulator Bi_2Se_3 thin film on a ferromagnetic insulating substrate

Shanna Zhu(朱珊娜), Gang Shi(史刚), Peng Zhao(赵鹏), Dechao Meng(孟德超), Genhao Liang(梁根豪), Xiaofang Zhai(翟晓芳), Yalin Lu(陆亚林), Yongqing Li(李永庆), Lan Chen(陈岚), Kehui Wu(吴克辉)

Chin. Phys. B . 2018, 27(7): 076801 . **doi:** 10.1088/1674-1056/27/7/076801

Segregations and desorptions of Ge atoms in nanocomposite $Si_{1-x}Ge_x$ films during high-temperature annealing

Yu Wang(汪煜), Meng Yang(杨濛), Gang Wang(王刚), Xiao-Xu Wei(魏晓旭), Jun-Zhuan Wang(王军转), Yun Li(李昀), Ze-Wen Zou(左则文), You-Dou Zheng(郑有炓), Yi Shi(施毅)

Chin. Phys. B . 2017, 26(12): 126801 . **doi:** 10.1088/1674-1056/26/12/126801

Structural characteristics of surface-functionalized nitrogen-doped diamond-like carbon films and effective adjustment to cell attachment

Liu Ai-Ping, Liu Min, Yu Jian-Can, Qian Guo-Dong, Tang Wei-Hua

Chin. Phys. B . 2015, 24(5): 056804 . **doi:** 10.1088/1674-1056/24/5/056804

Energy storage performances regulated by $BiMnO_3$ proportion in limited solid solution films*

Fei Guo(郭飞), Zhifeng Shi(史智锋), Yaping Liu(刘亚平), and Shifeng Zhao(赵世峰)†

School of Physical Science and Technology, Inner Mongolia Key Laboratory of Nanoscience and Nanotechnology, Inner Mongolia University, Hohhot 010021, *China*

(Received 4 April 2020; revised manuscript received 8 July 2020; accepted manuscript online 15 July 2020)

$Na_{0.5}Bi_{0.5}TiO_3$–$BiMnO_3$ (NBT–BM) limited solid solution films were fabricated to investigate the lattice modification on the energy storage performances. The introduction of the BM solute lattice induces the NBT solvent lattices undergoing the transition from the pure phase, solid solution, solubility limit to precipitation. Correspondingly, the polarization states transfer from the macroscopic ferroelectric domains to nanodomains then to compound ferroelectric domains. The introduction of $BiMnO_3$ generates great lattice changes including the local lattice fluctuation and the large lattice stretching, which enhance the energy storage performances, with the energy storage efficiency being enhanced from 39.2% to 53.2% and 51.7% and the energy density being enhanced from 33.1 J/cm^3 to 76.5 J/cm^3 and 83.8 J/cm^3 for the BM components of 2% and 4%, respectively. The lattice modifications play a key role in the energy storage performances for limited solid solution films, which provides an alternative strategy for energy storage material.

Keywords: limited solid solution, energy storage, relaxor, lattice engineering

PACS: 68.55.−a, 77.80.−e, 84.60.Ve **DOI:** 10.1088/1674-1056/aba604

1. Introduction

Dielectric capacitors have aroused wide excitements due to their superior performances in charge–discharge velocity and power density.[1–4] For them, the energy storage density (U_r) and efficiency (η) can be indirectly computed by the curves of polarization (P) vs. the electric field (E), which can be expressed as[5]

$$U_r = \int_{P_r}^{P_m} E \cdot dP, \tag{1}$$

$$\eta = \frac{U_r}{U} = \frac{U_r}{U_r + U_{loss}} \times 100\%, \tag{2}$$

where P_m and P_r are the maximum and remanent polarization, respectively. U_{loss} represents the energy dissipation. Therefore, the key factors for enhancing energy storage performances are to increase the polarization difference ($\Delta P = P_m - P_r$) and breakdown strength (E_{BDS}). Relaxor ferroelectric films become the most important candidates for energy storage due to the low P_r. Several efforts have been attempted to construct the relaxor ferroelectric films including doping or introducing a solid solution.[6,7] It would cause the disorder of A- or B-site cations or composition fluctuation, and then produce the random electric field, further destroying the original macroscopic ferroelectric domains to form polar nano regions (nanodomains).[8–10]

The solid solution materials are classified into two categories: the continuous solid solution at any soluble proportion, and the limited solid solution, in which one phase precipitates from the solid solution until the solute lattices exceed a certain proportion.[11] It is easy for the former to obtain relaxor behaviors by changing the phase structure. While for the latter, the complicated effects, which include not only the coupling effect between solvent and solute lattices, but also the phase precipitations, have a remarkable influence on the dipoles and lattices. Based on such complicated effect, we design a limited solid solution film of $(1-x)Na_{0.5}Bi_{0.5}TiO_3$–$xBiMnO_3$ (NBT–BM) with $x = 0, 0.02, 0.04, 0.06$. The lattice parameters of the solvent lattices (NBT) gradually increase as the solute lattices (BM), generating the local lattice fluctuation and distortion, which results in the films undergoing the transition from the pure phase, solid solution, solubility limit to the precipitation, accompanied by the transition from ferroelectric, relaxor ferroelectric to compound ferroelectric states. The local lattice fluctuation induces the relaxor behaviors and improved energy storage efficiency, and the lattice stretching at the solubility limit enhances the polarization, which enhances the energy storage densities by 153.2%. The mechanics of lattice modified energy storage performances dependent on the solubility limit are detailly discussed.

2. Experimental details

The NBT–BM limited solid solution films are prepared by the sol–gel method. $Mn(CH_3COO)_3 \cdot xH_2O$ (96.0%, Alfa Aesar) and $CH_3(CH_2)_3O]_4Ti$ (98.0%, Sinopharm Chemical Reagent Co., Ltd) are dissolved in 2-methoxyethannol to form solution A. $Bi(NO_3)_3 \cdot 5H_2O$ (99.0%, Alfa Aesar) and

*Project supported by the National Natural Science Foundation of China (Grant Nos. 11864028 and 11564028) and Inner Mongolia Science Foundation, China (Grant No. 2018MS01003).

†Corresponding author. E-mail: zhsf@imu.edu.cn

© 2020 Chinese Physical Society and IOP Publishing Ltd

CH_3COONa (99.0%, Alfa Aesar) are dissolved in ethylene glycol to form solution B. Then the solution A is dripped into the solution B to form a homogeneous precursor solution, which is coated onto Pt/Ti/SiO_2/Si(100) substrates. Finally, the films are dried at 350 °C and anneal at 620 °C under the oxygen atmosphere. The crystal structures are characterized using high-resolution transmission electron microscopy (HRTEM-FEI F20) and x-ray diffractometer (XRD, Panalytical Empyrean). The dielectric permittivity and loss are characterized by an impedance analyzer (Agilent E4990A). Hysteresis loops, leakage current, and Weibull distribution are measured by a radiant multiferroic tester system (RT-500).

3. Results and discussion

XRD patterns of the $(1-x)$NBT–xBM films with $x = 0$, 0.02, 0.04, 0.06 are shown in Fig. 1(a). The diffraction peaks are in agreement with the pseudo-cubic $Na_{0.5}Bi_{0.5}TiO_3$ (ICS card No. 192002), based on the space group of *Pm3m*. As more solid solution lattice (BM) is introduced, the diffraction peaks shift toward a lower 2θ angle until the BM phases precipitate at a solute proportion of 4%, which is identified as the solubility limit. The precipitation phases are indexed based on the monoclinic phase $BiMnO_3$ (ICS card No. 245299). Over this proportion, the peaks continue to shift toward a low angle and the peak intensity of the precipitation phase is strengthened. The enlarged image is shown in Fig. 1(b). It shows that the peak position obviously changes below the solubility limit. Above the solubility limit, the shift of diffraction peaks gets slow and the precipitation phase becomes more dominant. Detailed lattice parameters of the NBT–BM limited solid solution are investigated by Rietveld refinement, as shown in Table 1. The converged weighted R factors (wRp and Rp) and goodness-of-fit indicator (χ^2) reveal a good matching degree of the crystal structure. The lattice parameters (a, b, and c) gradually increase with the BM proportion, which also results in the expansion of the lattice volumes, as shown in Fig. 1(c). And NBT–BM solid solution films undergo the transition from the pure phase, solid solution, solubility limit, to precipitation.

Table 1. The refined XRD patterns of the NBT–BM limited solid solution.

	wRp	Rp	χ^2	$a=b=c$/Å	Volume/Å^3
NBT	8.3%	6.4%	1.204	3.8899	58.857
NBT–0.02BMO	8.9%	6.8%	1.291	3.9107	59.811
NBT–0.04BMO	7.4%	5.6%	1.251	3.9168	60.089
NBT–0.06BMO	8.2%	6.5%	1.463	3.9192	60.199

The lattice distortion is further confirmed by HRTEM images in Figs. 1(d)–1(g). As can be seen, the plane distance of the pure NBT films is 2.760 Å, as shown in Fig. 1(d), which corresponds to the (110) plane of pseudo-cubic NBT. With the increase of solute lattices (BM), the (110) plane distance increases to 2.763 Å at a solid solution proportion of 2%, as shown in Fig. 1(e). Further increasing the proportion of BM lattices, monoclinic BM phases with the (111) plane distance of 2.331 Å begin to precipitate over the solid solution proportion of 4%, as shown in Fig. 1(f). Further increasing BM proportion to 6%, more monoclinic BM phases precipitate, as shown in Fig. 1(g). That is to say, the NBT–BM film is a limited solid solution with a solubility limit of 4%. Interestingly, over the proportion of the solubility limit, the plane distance of the NBT lattices continues to increase because NBT solvent lattices are stretched by binding force when the BM lattices precipitate. Atomic force microscope (AFM) is an effective method for evaluating film quality at the nanoscale. Figure 2 displays the AFM surface morphology of $(1-x)$NBT–xBM limited solid solution films with $x = 0, 0.02, 0.04$, and 0.06. All samples present a highly smooth surface with the average surface roughness of 2.91 nm, 3.46 nm, 3.70 nm, and 2.54 nm, respectively.

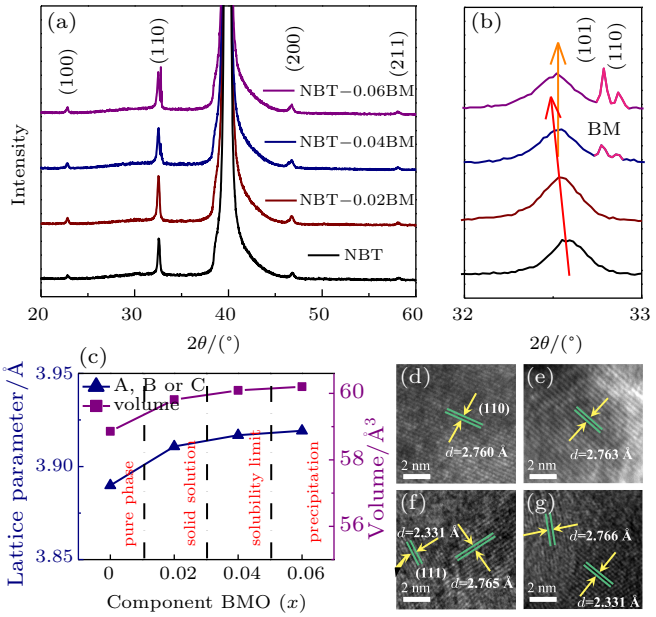


Fig. 1. (a) XRD patterns of NBT–BM limited solid solution films. (b) Enlarged XRD patterns. (c) Lattice parameters and the phase transition of limited solid solution. (d)–(g) HRTEM images of the $(1-x)$NBT–xBM limited solid solution with x equaling to 0, 0.02, 0.04, and 0.06, respectively.

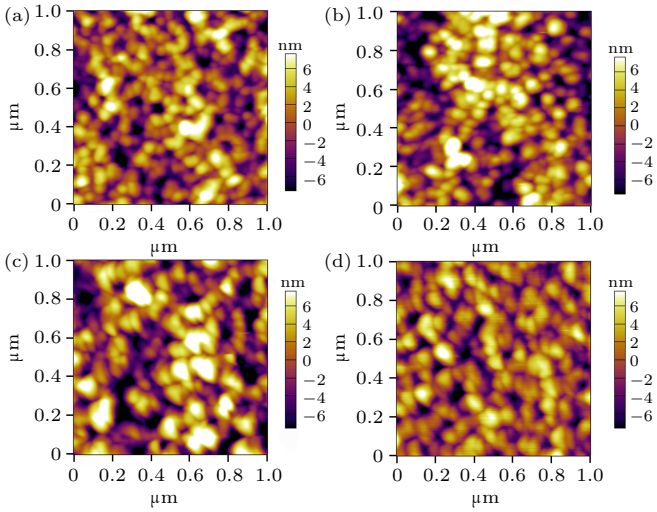


Fig. 2. AFM surface morphology of $(1-x)$NBT–xBM limited solid solution: (a) $x = 0$, (b) $x = 0.02$, (c) $x = 0.04$, (d) $x = 0.06$.

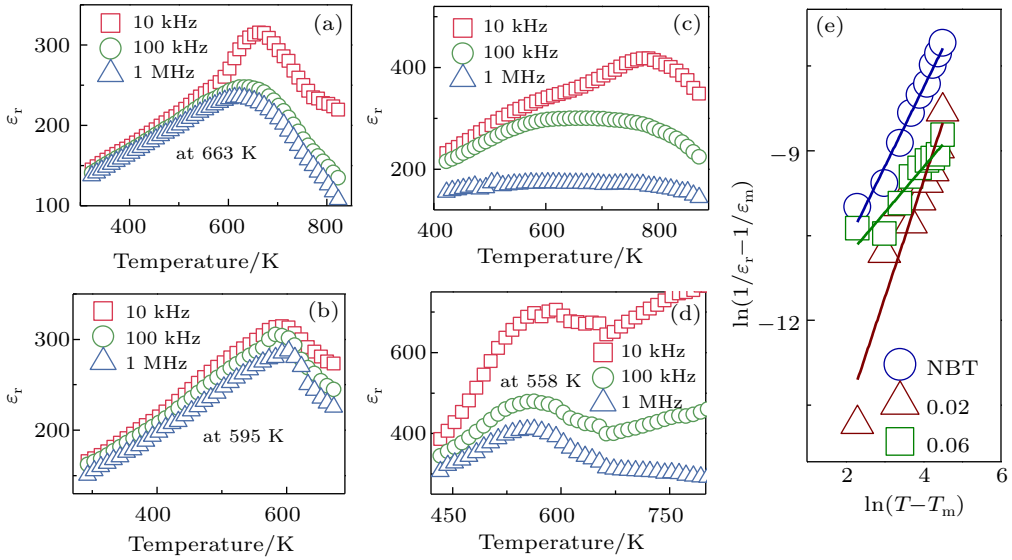


Fig. 3. (a)–(d) Temperature-dependent dielectric constants of the pure NBT, 0.98NBT–0.02BM, 0.96NBT–0.04BM, and 0.94NBT–0.06BM, respectively. (e) Dispersion coefficient γ of NBT–BM limited solid solution films.

The temperature-dependent dielectric constants are displayed in Fig. 3. As shown in Fig. 3(a), the pure NBT films present obvious dielectric peaks at the temperature of 663 K. While the 0.98NBT–0.02BM solid solution films display obvious diffuse peaks, and the peak shifts from 595 K towards high temperature with the increase of the frequency, as shown in Fig. 3(b), which are the important characteristics of relaxor ferroelectrics.[12] For the 0.96NBT–0.04BM films, at the solubility limit, as shown in Fig. 3(c), different from traditional ferroelectrics and relaxor ferroelectrics, there is no obvious phase transition emerging at high frequency. It reveals that the dual characteristics resulted from the NBT lattices and the precipitation at the solubility limit lead to the great difference in internal phase structure to weaken the phase transition, where it is defined as the composite ferroelectric states. However, above the solubility limit, the 0.94NBT–0.06BM films again show dielectric peaks at a temperature of 558 K, as shown in Fig. 3(d). Figure 3(e) displays the dispersion coefficient γ of the NBT–BM limited solid solution films at 10 kHz except for the 0.96NBT–0.04BM films. The γ value of 0.94NBT–0.06BM is measured around the peak of 558 K due to abnormal dielectric emerged above a temperature of 663 K. As shown, the γ values are 1.398, 2.069, and 0.804 for the pure NBT, 0.98NBT–0.02BM, and 0.94NBT–0.06BM films, respectively. It means that the pure NBT films are ferroelectric, and the 0.98NBT–0.02BM films present typical relaxor behaviors.[13] Besides, the 0.94NBT–0.06BM films show a high dielectric constant without frequency dispersion due to the lattice distortion and the precipitation, which means the composite ferroelectric states. Thus, with an increase in BM proportion, the limited solid solution films undergo the transition from ferroelectric, relaxor ferroelectric to composite ferroelectric states.

Figure 4(a) shows the *P*–*E* loops of the NBT–BM limited solid solution films with different BM components at 1198 kV/cm, where the electrode connection form is along the thickness with the test frequency of 1 kHz. As predicted, the *P*–*E* loops show the relaxor characteristics at the solute proportion of 2%. And at the solubility limit of 4%, the *P*–*E* loops show a larger polarization. When the proportion reaches 6%, the polarization turns to drop because the massive precipitations result in defects, which decreases the polarization. It is obvious that the coercive field decreases at the proportion of 2% and then increases with the increase of the BM component. However, both P_m and P_r drop at a proportion of 6% due to the massive defects. Figure 4(c) shows the leakage current curves under different components. The relaxor ferroelectric films show excellent leakage characteristics due to the depression of the electronic movement derived from the scattering of the local field.[14] Continuing to increase the BM component, the leakage currents gradually increase due to mobile electrons derived from the defects. Correspondingly, the breakdown strength characteristics are investigated by Weibull distribution.[15] As shown in Fig. 4(d), the breakdown strengths are 2252 kV/cm, 3708 kV/cm, 3041 kV/cm, and 2416 kV/cm for the BM components of 0%, 2%, 4%, and 6%, respectively. The tendency of breakdown strength is consistent with that of leakage current. Interestingly, the relaxor ferroelectric films endow the largest breakdown strength due to the excellent leakage characteristics. It is worth mentioning that the breakdown strengths for the BM components of 4% and 6% are larger than that of pure NBT films, which is different from the leakage characteristic. It is attributed to the fact that the Weibull distribution reveals the competitive relationship between the mobile charge concentration and interface scattering. The interfaces are generated due to the formation of solid solution and precipitation, which lead to an increase in the scattering center. The Weibull distributions are carried out at a high frequency of 1 kHz, which inhibits the mobile charges to form the current due to interface scattering. Thus,

the breakdown strengths for the BM components of 4% and 6% are larger than that of the pure NBT films. Moreover, the scattering with high frequency reduces the thermal loss accumulation around defects, which improves the breakdown characteristics.

Figure 5(a) displays the *P*–*E* loops near breakdown electric fields to compute the energy storage performances. The 0.98NBT–0.02BM films endow the largest breakdown strength, and the 0.96NBT–0.04BM films present the maximum polarization. As shown in Fig. 5(b), the recovery energy density of the pure NBT films is 33.1 J/cm^3. In contrast, the energy densities for relaxor films and solubility limit films show great improvement, which are as high as 76.5 J/cm^3 and 83.8 J/cm^3 with increase ratios of 131.1% and 153.2%, respectively. Increasing the BM over the solubility limit, the defects result in the decrease of the energy density to 46.7 J/cm^3. Similarly, the energy storage efficiency is obviously improved after introducing solution lattices, as shown in Fig. 5(c), where the efficiency is enhanced from 39.2% to 53.2%, 51.7%, and 55.6% near the breakdown electric field for the BM component of 0%, 2%, 4%, and 6%, respectively. The relaxor ferroelectric films present slightly higher energy efficiency than the solubility limit films due to their relaxor behaviors. While the solubility limit films show a larger energy density per unit electric field.

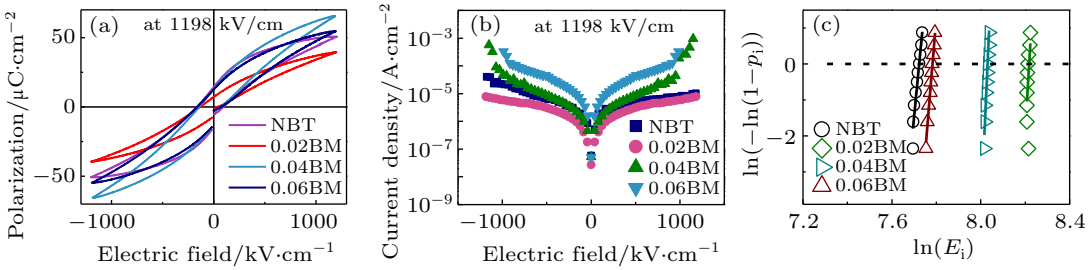


Fig. 4. (a) The *P*–*E* loops of the NBT–BM limited solid solution films at 1198 kV/cm. (b) The leakage current of the NBT–BM limited solid solution films. (c) Weibull distribution of breakdown strength for the NBT–BM limited solid solution films.

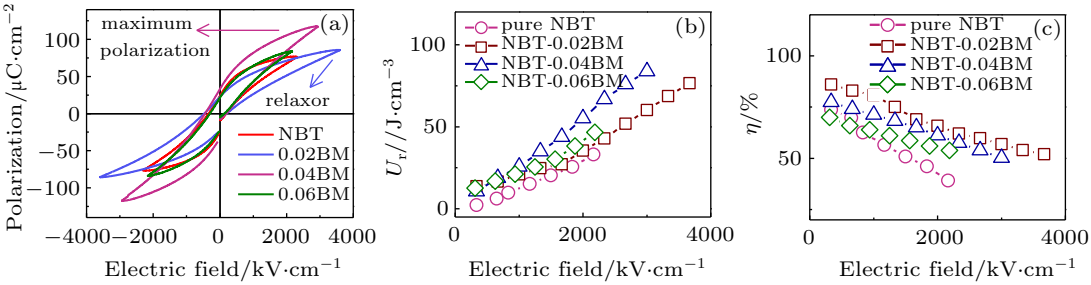


Fig. 5. (a) The *P*–*E* loops of NBT–BM limited solid solution films near the breakdown electric field. (b) The energy density. (c) The efficiency of NBT–BM limited solid solution films.

Obviously, the energy storage performances for the limited solid solution films are related to the ferroelectric properties, which are decided by the inner polarization states. Figure 6 schematically shows the lattice modification on the polarization states. As shown in Fig. 6(a), the possible spontaneous polarization directions for the NBT solvent lattices are along the body-centered diagonal.[16] In the two-dimensional {110} crystal plane, the NBT lattices show unitary consistency, as shown in Fig. 6(b). The polarization is considered as the softening of the lattice waves at the center of the Brillouin zone resulted from the forced vibrations,[17]

$$\varepsilon = 1 + \frac{N \cdot q^2 \cdot m}{w_j^2}, \tag{3}$$

where m, N, w_j, q, and ε are the effective mass, the number of displaced charges in unit volume, lattice wave frequency, the charge of displacement ion, and dielectric constant, respectively. When the frequency of one specific optical module drops to near 0, the separation of positive and negative charges at the Brillouin zone gives rise to the polarization, as shown in Fig. 6(c). Meanwhile, the strong coupling between dipoles derived from unitary consistency crystal results in the macroscopic polarization regions in the pure NBT lattices, as shown in Fig. 6(d). Thus, ferroelectric states are formed.

For the 0.98NBT–0.02BM solid solution films, the solute lattices enter into the NBT lattices, as shown in Fig. 6(e). The corresponding crystal structure is sketched by two-dimensional {110} crystal plane in Fig. 6(f). It is suggested that the lattices are distorted due to the difference in ion radius. Meanwhile, the lattices fluctuate at local regions since the moderate solute lattices entered into solvent lattices change the local structure including the atomic density and Coulomb interactions. And the local effect is stronger than that of lattice distortion due to intense interaction and interface segmentation induced local field. Therefore, it would be fluctuated for the separation states of the positive and negative charges at the Brillouin zone, as shown in Fig. 6(g). Moreover, the local

lattice fluctuation generates the polarization fluctuation, which enhances the potential barrier for the lattice waves and results in a rapid increase of the vibration restoring force and the decrease of the dielectric constant according to Curie–Weiss law[18]

$$\varepsilon = 1 + \frac{N \cdot q^2/K}{T - T_0}, \tag{4}$$

where K, T, and T_0 are the equivalent force constant, external temperature, and Curie temperature, respectively. Thus the high potential barrier produces the random field at local regions, which weakens the interaction among dipoles, destroys the crystal long-range order, and divides the macroscopic domains into polar nano regions to form relaxor ferroelectric states, as shown in Fig. 6(h). Fortunately, the mobile electrons are scattered by the random field, which is the reason why the relaxor ferroelectric films are endowed with the excellent leakage characteristics and high breakdown strength.

Further increasing the solute lattices (BM) to reach the solubility limit for the 0.96NBT–0.04BM films, generating lattice mismatching, the BM phases begin to precipitate, as shown in Fig. 6(i). Interestingly, the precipitations still have an influence on the lattice stretching due to the binding force of the ionic bond.[19] Figure 6(j) shows such lattice distortion in two-dimensional {110} plane, where the precipitations different from the host lattices are obtained, and the ionic bonds still stretch the lattice, resulting in the large lattice distortion. Figure 6(k) schematically displays the displacement of the charge for the 0.96NBT–0.04BM films at the solubility limit. The lattice distortion intensifies the relative displacement of positive and negative charges at the Brillouin zone and enhances the polarization. Thus, the composite domains including the ferroelectric and relaxor ferroelectric domains have been obtained because the local lattice fluctuation is weakened and the lattice stretching is improved, as shown in Fig. 6(l). It is worth noting that the lattice distortion and local lattice fluctuation have great impacts on the ferroelectric characteristic. After few amounts of solute lattices are introduced into host lattices, the great difference between solute lattices and solvent lattices results in the intense local lattice fluctuation, which is stronger than the influence of lattice distortion due to the local interaction. However, when the solute lattice exceeds certain amounts, the local effect would be weakened and the ferroelectric domains would be rebuilt, which suppresses the relaxor characteristics and results in abnormal relaxor behaviors.[14,20]

With the further increase of the BM content in the $(1-x)$NBT–xBM solid solution, the precipitation of the massive BM phases leads to more internal defects such as vacancies, as shown in Fig. 6(m). The corresponding crystal structure in the {110} plane is shown in Fig. 6(n). Although the lattice stretching still increases the relative displacement of positive and negative charges at the Brillouin zone, more defects reduce massive displaced charges in unit volume, which weakens both the polarization and dielectric endurance, as shown in Fig. 6(o). The corresponding domain structure is shown in Fig. 6(p), and it reveals that lots of precipitations and defects result in the decrease of the polarization.

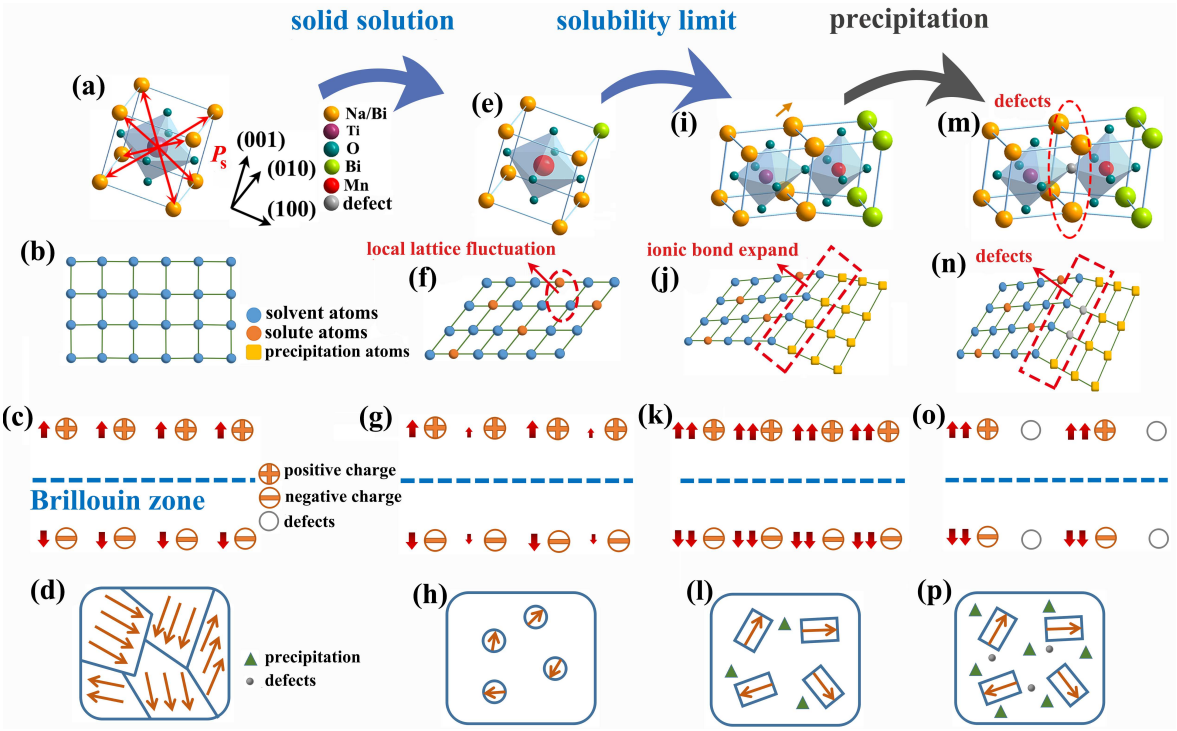


Fig. 6. The schematic diagram of polarization states modulated by the lattice engineering: (a), (e), (i), and (m) The crystal structure of the NBT, 0.98NBT–0.02BM solid solution, 0.94NBT–0.06BM at the solubility limit, and 0.94NBT–0.06BM with precipitations, respectively. (b), (f), (j), and (n) The lattices of the NBT, 0.98NBT–0.02BM solid solution, 0.96NBT–0.04BM, and 0.94NBT–0.06BM in two-dimensional {110} crystal plane, respectively. (c), (g), (k), and (o) The schematic diagram of charge displacement for the NBT, 0.98NBT–0.02BM solid solution, 0.96NBT–0.04BM, and 0.94NBT–0.06BM lattices at the Brillouin zone, respectively. (d), (h), (l), and (p). The domain structure diagram of the pure NBT, 0.98NBT–0.02BM solid solution, 0.96NBT–0.04BM, and 0.94NBT–0.06BM, respectively.

4. Conclusions

In summary, the lattice modification plays a key role in the energy storage performances for the NBT–BM limited solid solution films. With the increase of the solute lattices proportion, the lattice undergoes the transition process from the pure phase, solid solution, solubility limit to precipitation for the BM component of 0%, 2%, 4%, and 6%. Correspondingly, the polarization states transform from single ferroelectric, relaxor ferroelectric to compound ferroelectric states. Such evolvement of the polarization states is attributed to the lattice modification including the local lattice fluctuation and lattice stretching. The relaxor behaviors are attributed to the local lattice fluctuation and the lattice waves with the enhanced potential barrier, which leads to intense interaction and interface segmentation to induce the local field. Besides, the large polarization characteristics could be induced by large lattice distortion with precipitation of ionic bonds displayed by the 0.96NBT–0.04BM films. By the lattice modification, the energy storage efficiency is enhanced from 39.2% to 53.2% and 51.7% for BM components of 2% and 4%, and the energy density has been enhanced from 33.1 J/cm^3 to 76.5 J/cm^3 and 83.8 J/cm^3 for BM components of 2% and 4%, respectively, which provides an alternative design strategy for the energy storage in solid solution materials.

References

[1] Zhang X, Shen Y, Xu B, *et al.* 2016 *Adv. Mater.* **28** 2055
[2] Liu C, Li F, Ma L P, *et al.* 2010 *Adv. Mater.* **22** 8
[3] Zuo Z H, Zhan Q F, *et. al.* 2016 *Chin. Phys. B* **25** 087702
[4] Chu B, Zhou X, Ren K, *et al.* 2006 *Science* **313** 334
[5] Yao Z. H, Song Z, Hao H, *et al.* 2017 *Adv. Mater.* **29** 1601727
[6] Pan H, Zheng Y, Shen Y, *et al.* 2017 *J. Mater. Chem. A* **5** 5920
[7] Wang G, Li J L, Zhang X, *et al.* 2019 *Energy Environ. Sci.* **12** 582
[8] Cross L E 1987 *Ferroelectrics* **76** 241
[9] Thomas N W 1990 *J. Phys. Chem. Solids.* **51** 1419
[10] Chen C W, Xiang Y, Tang L G, *et al.* 2019 *Chin. Phys. B* **28** 127702
[11] Xu K C and Chen Y 1999 *J. Raman Spectrosc.* **30** 441
[12] Birks E, Dunce M, Lgnatans R, *et al.* 2016 *J. Appl. Phys.* **119** 074102
[13] Cui L, Hou Y D, Wang S, *et al.* 2010 *J. Appl. Phys.* **107** 054105
[14] Guo F, Jiang N, Yang B, *et al.* 2019 *Appl. Phys. Lett.* **114** 253901
[15] Kishimoto A, Koumoto K and Yanagida H 1989 *J. Mater. Sci.* **24** 698
[16] Kitanaka Y, Noguchi Y, Miyayama M, *et al.* 2013 *Ferroelectric* **443** 1
[17] Fokam J M 2008 *Commum. Math. Phys.* **283** 285
[18] Pra P D, Fischer M and Regoli D 2013 *J. Stat. Phy.* **152** 37
[19] Kaya S, Chamorro E, Petrov D, *et al.* 2017 *Polyhedron* **123** 411
[20] Ogihara H, Randall C A and McKinstry T S 2009 *J. Am. Ceram. Soc.* **92** 110